

RESEARCH ARTICLE

10.1002/2016JB012840

Key Points:

- We develop a new method (hypoRelocate) for high-resolution event relocation
- Stacked coda cross-correlograms are introduced as a new type of constraint
- HypoRelocate improves precision of event location over traditional methods

Correspondence to:

L. Sun,
sunli831022@gmail.com

Citation:

Sun, L., M. Zhang, and L. Wen (2016), A new method for high-resolution event relocation and application to the aftershocks of Lushan Earthquake, China, *J. Geophys. Res. Solid Earth*, 121, doi:10.1002/2016JB012840.

Received 21 JAN 2016

Accepted 20 MAR 2016

Accepted article online 5 APR 2016

A new method for high-resolution event relocation and application to the aftershocks of Lushan Earthquake, China

Li Sun^{1,2}, Miao Zhang¹, and Lianxing Wen^{1,3}

¹Laboratory of Seismology and Physics of Earth's Interior; School of Earth and Space Sciences, University of Science and Technology of China, Hefei, China, ²China Earthquake Networks Center, Beijing, China, ³Department of Geosciences, State University of New York at Stony Brook, Stony Brook, New York, USA

Abstract We develop a new method (named hypoRelocate) to determine high-resolution earthquake location, utilizing traditional constraints of absolute travel time and differential travel time, and one new constraint of coda cross-correlogram between the events. The relocation is performed by using a simulated annealing method to search for the best fitting locations and origin times of the events that minimize the total residual of the all above three constraints of the events. HypoRelocate expands the advantage of using differential constraints to better determine high-resolution relative locations between the events by constructing constraint of coda cross-correlograms on interevent distance and reduces the dependence of relocation results on the accuracy of the initial catalog by incorporating the absolute time into the joint inversion. The method is applied to relocate the aftershocks of Lushan Earthquake. The comparisons of the relocation results between hypoRelocate and hypoDD indicate that the additional constraints of coda cross-correlogram and absolute travel time place better constraints on relative location between the events and absolute location of the events.

1. Introduction

Determining high-resolution event location is important to the understanding of tectonics [Hauksson et al., 2012], fault zone structure [Rubin et al., 1999; Waldhauser and Ellsworth, 2000; Shearer et al., 2005; Schaff and Richards, 2004], rupture mechanism [Rubin, 2002], and evolution process of large earthquakes [Bouchon et al., 2011; Kato et al., 2012]. It also becomes an effective tool for monitoring velocity variations [Poupinet et al., 1984; Bokelmann and Harjes, 2000; Furumoto et al., 2001; Long and Wen, 2012] and volcano activities [Ratdomopurbo and Poupinet, 1995; Martini et al., 2009; Matoza et al., 2013] and evaluating the safety of the induced seismicity in many engineering operations [Talwani and Acree, 1984; Simpson et al., 1988; Rutledge and Phillips, 2003; Majer et al., 2007; Ellsworth, 2013]. The accuracy of absolute location determination would depend on seismic station coverage, the accuracy of travel time measurement, and the resolution of the seismic model used in the relocation [e.g., Pavlis, 1992; Gomberg et al., 1990]. Thus, efforts to improve the resolution of event location determination have been on many fronts: from the improvement of the accuracy of the seismic model used in the relocation [e.g., Husen and Smith, 2004; Hauksson and Shearer, 2005; Shearer et al., 2005; Lin et al., 2007] to the development of the methods of determining the relative location of the events using travel time difference between the events and to the increase of the accuracy of relative travel time measurement by waveform cross correlation [e.g., Waldhauser and Ellsworth, 2000; Richards-Dinger and Shearer, 2000; Schaff and Richards, 2004; Lin and Shearer, 2005; Wen, 2006; Waldhauser and Schaff, 2008; Wen and Long, 2010; Zhang and Wen, 2013]. So far, the methods of using travel time difference between the events to determine the relative location of the events [Waldhauser and Ellsworth, 2000; Richards-Dinger and Shearer, 2000; Lin and Shearer, 2005; Wen, 2006] have provided the highest resolution for the relative locations of the events, although the resolution of the absolute event location obtained from those methods would still depend on the accuracy of the initial catalog.

In this paper, we develop a new method (we name it hypoRelocate) for high-resolution earthquake relocation, which incorporates constraint of stacked coda cross-correlogram along with absolute travel time and differential travel time. HypoRelocate constructs new additional constraints on interevent distance based on stacked coda cross-correlogram, retains the advantage of using travel time difference to better constrain the relative location between events, and reduces the dependence of relocation result on catalog absolute location by

combing absolute travel time. In this study, we present the concept of stacked coda cross-correlogram as new constraint in section 2, the procedures of hypoRelocate in section 3, the application to the determination of the aftershock locations of Lushan earthquake in section 4, and the comparison with another high-resolution relocation method hypoDD [Waldhauser and Ellsworth, 2000] in section 5.

2. Coda Cross-Correlogram Between Events as Constraint on Interevent Distance

HypoRelocate employs a new type of constraint on interevent distance based on stacked coda cross-correlogram. The constraint is an extension of the applications of seismic interferometry in earthquake seismology. In this section, we introduce its concept and present synthetic validations.

In recent years, seismic interferometry has been, in many aspects, applied to earthquake seismology. The applications can be classified into two categories: (1) approximate Green's functions of surface and body waves between two stations have been successfully extracted from the correlation of seismic coda [Campillo and Paul, 2003] or ambient seismic noise [Shapiro *et al.*, 2005; Roux *et al.*, 2005; Miyazawa *et al.*, 2008], and (2) by reciprocity, approximate Green's functions of seismic fields have also been extracted between seismic sources from the correlation of seismic data between the sources [Curtis *et al.*, 2009; Galetti and Curtis, 2012; Tonegawa and Nishida, 2010; Poliannikov *et al.*, 2011; Zhang *et al.*, 2014].

The constraint on interevent distance based on stacked coda cross-correlogram employs seismic interferometry by reciprocity. According to Curtis *et al.* [2009], approximate Green's function of seismic fields (strain or strain rate) between two subsurface earthquakes could be derived by summing cross-correlograms of seismic data between the events over an enclosed distribution of receivers. Based on this theory, the integration (stacking) of cross correlations of seismic coda waves over an enclosed distribution of receivers would represent an approximate Green's function from the one earthquake source to the other, which would contain the travel time information from one source to the other and can be used to place constraint on interevent distance. Using seismic coda waves would further relax the requirement of station distribution to extract the Green's functions based on interferometry, as the strong scattering would generate seismic scattering energy that radiates from various directions from the sources into the diffuse coda wave field [Aki, 1969; Aki and Chouet, 1975; Hoshiba, 1991] and effectively improves the seismic station coverage [Snieder *et al.*, 2002; Snieder, 2002, 2004, 2006; Campillo and Paul, 2003].

We use a series of 2-D SH (*S* waves polarized in the horizontal plane) velocity synthetic examples to demonstrate the validity of the above inference. In the examples, we generate SH coda waves with a two-layer model with randomly distributed scatterers by a 2-D finite difference method, construct coda wave cross-correlograms between the events, and compare the travel time information of the cross-correlograms with source parameters. All velocity models extend 40 km in the horizontal direction and 40 km in depth, with a background SH velocity of 3.5 km/s in the first layer and 4.0 km/s in the second layer. The grid spacing of the finite difference calculation is 20 m in both horizontal and vertical directions, and the sampling time interval is 0.002 s. The source time function is a Ricker wavelet with a dominant frequency of 8 Hz. Fifty-nine stations are evenly located at the surface within an epicentral distance range from -5.8 km to 5.8 km (Figure 1a).

We test two scattering models and various combinations of source types. The first scattering model includes 1000 scatterers randomly distributed in the first layer, with randomly perturbed velocities from -30% to $+30\%$ and radii from 0 to 0.2 km (Figure 1a). We term it the even scattering model for discussion purpose. The second scattering model is an uneven scattering model with scatterers located on the left side of the model only (Figure 2a).

We first present an example of coda wave cross-correlograms of the even scattering model for two strike-slip (SS) faults, located at 1 km deep and separated by 1 km. We cross-correlate the synthetic coda seismograms from 2 to 4 s after the direct SH waves of the two events (Figure 1b) and then stack the normalized cross-correlograms of the coda waves (Figure 1c). The cross correlation is conducted in the frequency domain with no spectral balancing. Two clear spike phases are visible at ± 0.286 s in the stacked cross-correlogram (Figure 1d). Based on the background velocity of 3.5 km/s, we recover the traveling distance of 1 km based on the time separation between the stacked energy peaks (i.e., 3.5 km/s multiple 0.286 s), which is equal to the actual separation of the two sources. Thus, the emergence of these energy peaks in the stacked coda cross-correlogram and the time separation between them support the inference that the stacked cross-

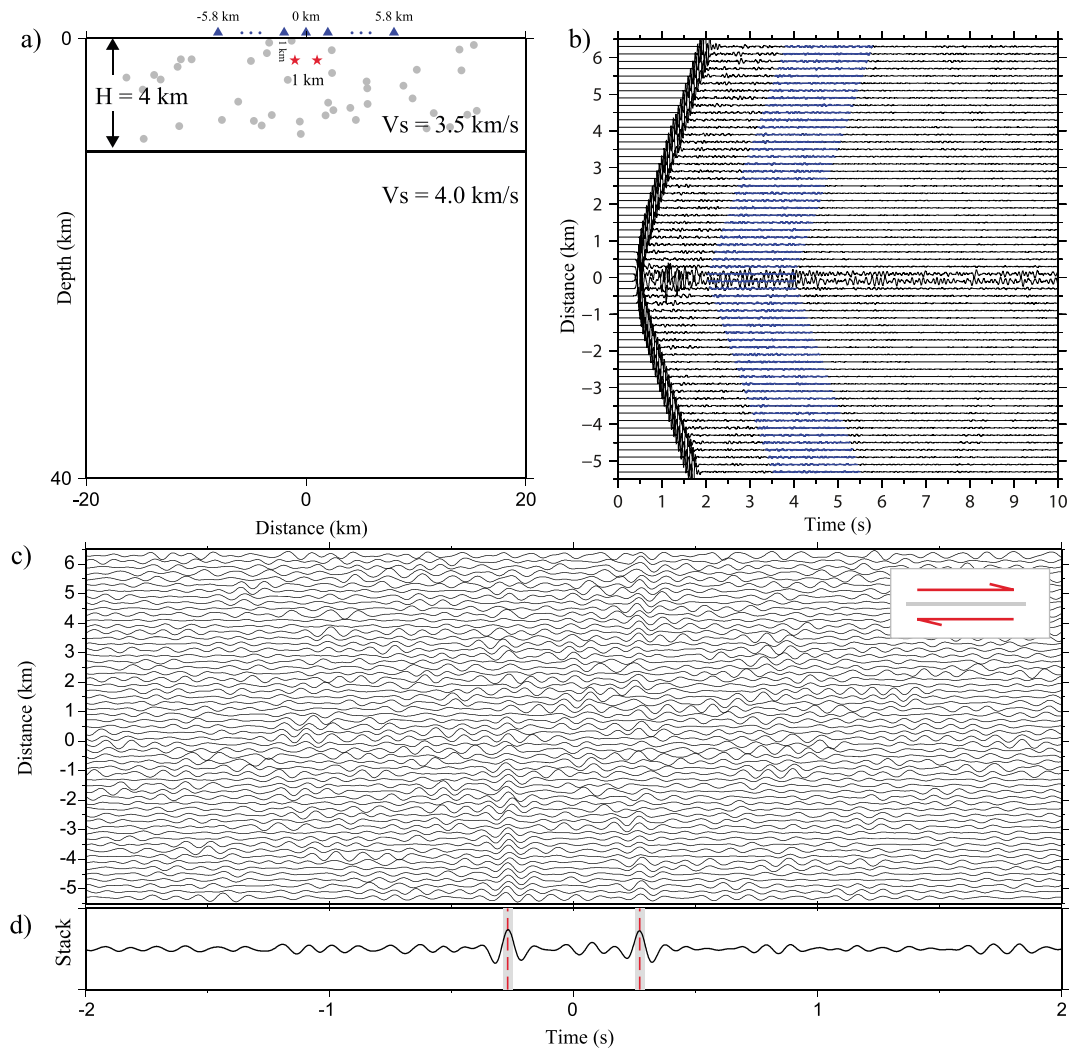


Figure 1. Stacked synthetic coda cross-correlogram and its relationship with event separation, for a model with randomly distributed scatterers. (a) Model of scatterers (gray points) used in 2-D SH coda wave synthetics calculation, 59 stations (blue triangles, evenly distributed on the surface) and earthquake sources (red stars). Earthquake sources are two strike-slip faults, located at 1 km in depth and separated by 1 km. Scatterers are randomly distributed with velocity perturbations varying from -30% to 30% and radii from 0 to 0.2 km. The background velocities are 3.5 km/s and 4.0 km/s for the first and second layers, respectively. (b) SH synthetic seismograms calculated for the source in Figure 1a, based on the stations and model in Figure 1a. Blue shadowed region shows the time window for constructing the coda-correlograms in Figure 1c. (c) Coda wave cross-correlograms obtained by correlating the coda waves for the source in the left to those for the source in the right in Figure 1a. (d) Cross-correlogram stacked from those in Figure 1c, with the synthetic travel time between two sources marked by red dash lines.

correlogram of the coda waves is an approximate Green's function (strain rate) between the sources. Although *Curtis et al.* [2009] showed that the waveform shapes of the approximate Green's functions involve convolutions of source time functions of the events, which may or may not be zero phase. We suppose the effect of source time functions is minor in affecting the travel time pick of the stacked cross-correlograms in reality.

Additional synthetic tests indicate that the characteristics of the stacked coda cross-correlogram would be affected by the spatial distributions of seismic scatterers, event focal mechanisms, and relative orientation of the event pair. For example, when the scatterers are only located in one side of the event pair (Figure 2a), coda waves are more prominently present at the stations in the left side of the sources (Figure 2b). In this case, only

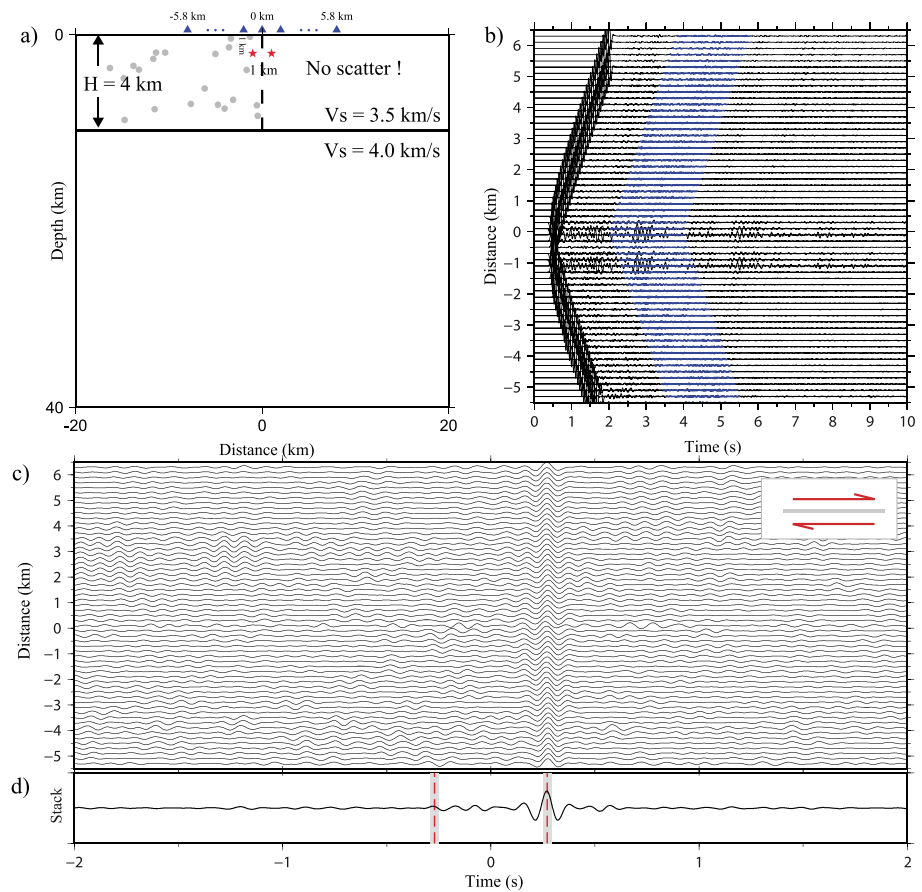


Figure 2. Same as Figure 1, except that the model has unevenly distributed scatterers (gray points), located only on the left side of the event pair.

one clear spike phase appears at 0.286 s in the cross-correlograms of individual station (Figure 2c) and the stacked coda cross-correlogram (Figure 2d).

To illustrate the effects of focal mechanism and relative orientation of the event pair, we show examples of the stacked coda cross-correlogram for various pairings of three fundamental faults: SS, vertical dip slip (DS) and 45° dip slip (45DS) for even scattering model in Figure 1. When the event pair are located at the same depth, the stacked coda cross-correlograms exhibit sharp spiking energy for three event pairings: SS versus SS, 45DS versus SS, and 45DS versus 45DS but no visible phase for other combinations of focal mechanisms (Figure 3a). However, when one source is placed 0.6 km deeper, the spiking energy now emerges in the stacked coda cross-correlograms for the event pairings of SS versus SS, DS versus SS, and DS versus DS (Figure 3b). Unlike the case that two sources are located at the same depth, spiking energy is no longer visible for 45DS versus SS and 45DS versus 45DS. Besides, the polarity of spike of DS versus SS is reverse, but the timing between them is the same as other two positive pairs. These results can be explained by the radiation patterns and relative orientation between the event pair. When two sources are located at same depth, SS and 45DS would radiate strong SH energy in the horizontal direction that links the two sources, while DS would do so in vertical direction. In the case that the sources are located at different depths, SS and DS would radiate strong energy along the direction between the two sources. In another word, when the focal mechanisms of the two sources would favor radiating strong energy along the direction between the two sources, clear spiking energy would emerge in the stacked coda correlogram.

The above synthetic tests support the inference that the stacked cross-correlogram of the coda waves is an approximate Green's function between the sources. It is also clear that direct S wave between two sources dominates over other potential phases in the stacked coda correlogram, for all the cases studied (Figures 1–3). The synthetics tests further suggest that the stack coda cross-correlogram may exhibit no

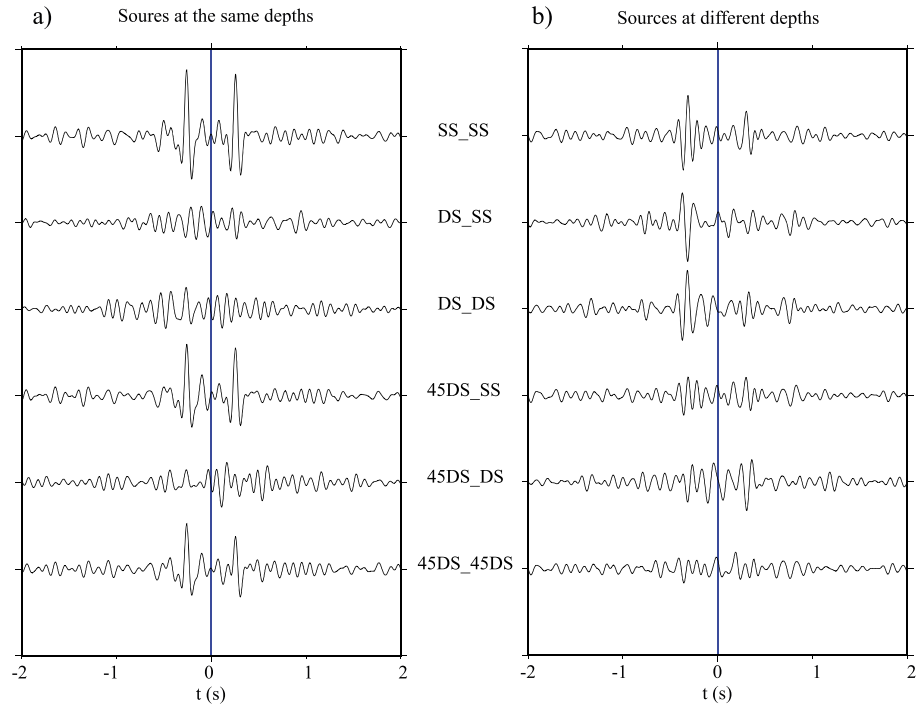


Figure 3. Stacked synthetic coda cross-correlograms of six event pairs with various focal mechanisms between them, for even scattering model in Figure 1 and two cases of source distribution: (a) both sources at 1 km depth (same as in Figure 1) and (b) two sources at 1 and 1.6 km depths. Each cross-correlogram is labeled with the types of earthquake focal mechanism between the event pair (with DS for dip-slip fault, SS for strike-slip fault, and 45DS for 45° dip-slip). The blue lines mark the zero time.

energy peak, one energy peak, or two symmetric energy peaks, depending on seismic scattering model, focal mechanisms of the pairing events, interevent distance, and relative orientation between the source locations. Despite the above complications, when energy peak(s) emerges in the stacked coda cross-correlogram, the timing of the peak(s) can be used to place constraint on the interevent distance between the events.

3. Methodology

HypoRelocate uses three types of constraint in relocation, including (1) absolute travel time of seismic phase, (2) differential travel time between the events, and (3) coda cross-correlogram between the events. The procedure of HypoRelocate method is illustrated schematically in Figure 4. The first step of the method is to build the three types of constraints for the events to be relocated, including (1) measuring absolute travel time and differential travel time from traditional means (catalog or waveform cross correlation) for all the events and (2) constructing coda cross-correlograms from a small set of events that have relatively larger magnitudes. For discussion purpose, we term these larger events as reference events. The second step is the utilization of the simulated annealing method to search for the best fitting locations and origin times of events that minimize the total residual of all the events that is defined by the difference between the observation and prediction of the three types of constraints. In the following subsections, we discuss the definition of total residual, relationship of the residual to event parameters, relocation error, and detailed procedure of the simulated annealing method.

3.1. Total Residual and Its Relationship to Event Location and Origin Time

We define the total residual ΔT^{res} as a weighed combination of residuals of absolute travel time, differential travel time, and coda cross-correlogram travel time:

$$\Delta T^{res} = w_1 * \sum_i^N \Delta T_{i,a} / N + w_2 * \sum_{i,j}^M \Delta T_{i,j,r} / M + w_3 * \sum_{i,j}^Q \Delta T_{i,j,c} / Q \quad (1)$$

Relocation procedures of hypoRelocate

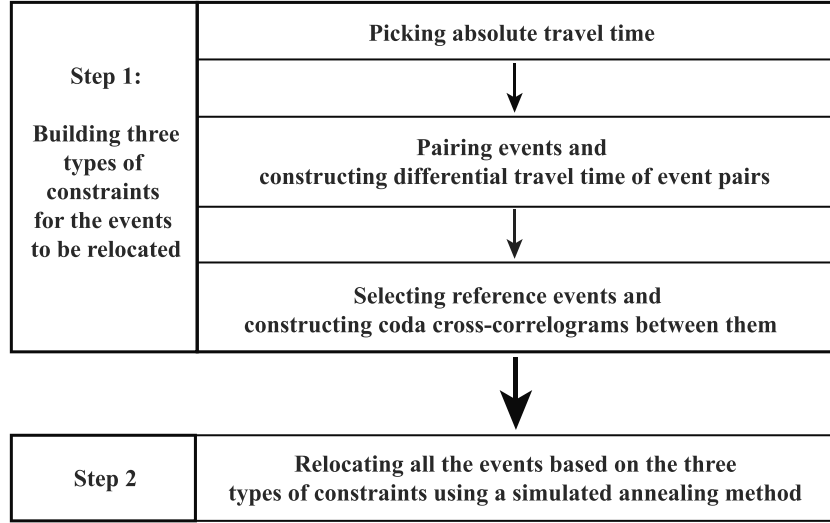


Figure 4. Relocation procedure of hypoRelocate.

where $\Delta T_{i,a}$ is the absolute time residual of event i , $\Delta T_{i,j,r}$ is the residual of travel time difference between event pair i, j , $\Delta T_{i,j,c}$ is the residual related to the stacked coda cross-correlogram between event pair i, j , N is the total number of events, M is the number of event pairs with the differential travel time constraints, Q is the number of coda cross-correlogram pairs, and w_1, w_2 , and w_3 ($w_1 + w_2 + w_3 = 1$) are the weighting factors for absolute travel time, differential travel time, and coda cross-correlogram, respectively.

The parameters to be inverted consist of the location (latitude, longitude, and depth) and origin time of each event. We describe below how each type of the residual is related to the observations and model parameters.

Let t_{ij}^{coda} be the measured time lag of the emerging energy in the stacked coda cross-correlogram; dL is the inter distance between the events calculated by events latitude, longitude, and depth; and v is the SH crustal velocity in the neighbor of event sources. When two symmetric energy peaks appear in the cross-correlograms, t_{ij}^{coda} is measured as the half of the time separation of the energy peaks, and coda time residual is defined as

$$\Delta T_{i,j,c} = \left| t_{ij}^{coda} - dL/v \right| \tag{2}$$

When only one energy peak is observed in the stacked cross-correlogram (Figures 2 and 3 for synthetic examples and Figure 9 for data examples), t_{ij}^{coda} is measured as the time lag of the energy peak from zero (could be positive or negative, depending on the side of the emerging energy from zero time). In that case, the measured time of the cross-correlogram peak would also depend on the assumed event origin time difference between the event pair. If event i is cross-correlated with event j , coda time residual for this case is defined as

$$\Delta T_{i,j,c} = \left| \left| t_{ij}^{coda} + \Delta O_{i-j} \right| - dL/v \right| \tag{3}$$

where ΔO_{i-j} is origin time difference correction between the event pair i, j that is caused by event origin time error and will be corrected in relocation as $\Delta O_{i-j} = \Delta O_i - \Delta O_j$, ΔO_i and ΔO_j are origin time corrections for event i and j , respectively.

Let $\Delta t_{i-j,k,p}$ be the travel time difference recorded at station k between event pair i, j for seismic phase p . It can be expressed as [Wen, 2006; Long and Wen, 2012; Zhang and Wen, 2013]:

$$\Delta t_{i-j,k,p} = dD_k * (dt/dD)(k, p, D, h) + dh * (dt/dh)(k, p, D, h) \tag{4}$$

where dD_k is the difference in epicentral distance at station k due to the relative difference in event location between the two events, dh relative change of event depth between the two events, and $(d/dD)(k, p, D, h)$, $(d/dh)(k, p, D, h)$ the derivatives of travel time (slowness) of the seismic phase with respect to epicentral distance D and event depth h , respectively.

Let $T_{i-j,k,p}^{\text{obs}}$ be the observed arrival time difference between events i and j for seismic phase p , the travel time difference residual $T_{i-j,k,p}^{\text{res}}$ is defined as

$$T_{i-j,k,p}^{\text{res}} = T_{i-j,k,p}^{\text{obs}} - (\Delta O_{i-j} + \Delta t_{i-j,k,p}) \quad (5)$$

and the total travel time difference residual of an event pair is defined as

$$\Delta T_{ij,r} = \sqrt{\sum_{k=1}^K \sum_{p=1}^P (\Delta T_{i-j,k,p}^{\text{res}})^2 / W} \quad (6)$$

P is the number of seismic phases of one station, K the number of stations, and W the total number of seismic phases used in the relocation.

The absolute time residual $\Delta T_{i,a}$ of event i is defined as

$$\Delta T_{i,a} = \sqrt{\sum_{k=1}^K \sum_{p=1}^P (\Delta T_{i,k,p}^{\text{res}})^2 / W} \quad (7)$$

$\Delta T_{i,k,p}^{\text{res}}$ is defined as $\Delta T_{i,k,p}^{\text{res}} = T_{i,k,p}^{\text{obs}} - \Delta O_i - t_{i,k,p}$, where $t_{i,k,p}$ is predicted travel time of p phase of event i at station k based on a reference model and $T_{i,k,p}^{\text{obs}}$ the observed travel time.

3.2. Event Relocation by the Simulated Annealing Method

As hypoRelocate combines different kinds of constraints in the relocation and some model parameters do not have linear dependence on the objective function, it becomes impossible to apply traditional iterative methods to find an optimal solution. Because of the large number of event parameters in the inversion, it is also impractical to apply grid search for seeking the best fitting model parameters. In hypoRelocate, we use the simulated annealing method to search for the best fitting locations and origin times of all the events that generate the minimal total residual of the events as defined in equation (1). Simulated annealing method is a probabilistic method for effectively solving the global optimization problem [Van Laarhoven and Aarts, 1987; Szu and Hartley, 1987; Goffe et al., 1994]. The method finds a solution that minimizes a particular objective function, through an iterative procedure controlled by the annealing schedule, specified by initial value, cooling rate, and acceptance probability. In this particular application, initial value defines initial searching area for event locations and searching time window for event origin times, cooling rate controls the speed of the decrease of the searching area and time window in each iteration, and the probability regulates whether a value should be accepted and the search goes to next iteration. The exact relocation procedure includes following steps:

1. Set $C = C_0$, where C and C_0 are the current event parameters and initial catalog values, respectively; S_0 be the initial searching area for event locations and searching time window for event origin times.
2. For each iteration i , $i = 1 \dots N_{\text{max}}$, where i is iteration index and N_{max} is the maximal number of iteration, the procedure chooses a set of new model parameter C_{new} , which is a random neighbor of C . The current searching range S decreases to $S = S_0 * (f)^i$, where f is the cooling rate with a value between 0 and 1. If $R(C_{\text{new}}) < R_{\text{min}}$ or $\exp(R_{\text{min}} - R(C_{\text{new}}))/S > \text{random}(0, 1)$, C_{new} is accepted as C and the procedure goes to next iteration; otherwise, it picks another random neighbor of C and repeats the procedure. Where R_{min} is the minimal residual of last iteration and $R(C_{\text{new}})$ is the residual of current model parameters C_{new} , $\text{random}(0, 1)$ gives a random decimal between 0 and 1. $\exp(R_{\text{min}} - R(C_{\text{new}}))/S > \text{random}(0, 1)$ is a probability condition to avoid the searching falling into a local minimal value.
3. The model space C and the associated minimal residual R_{min} in the last iteration are considered as the best fitting model and its associated residual.

3.3. Uncertainty Estimates of Relocation Results

Relocation uncertainty of an individual event (e.g., event i) is estimated based on statistical analysis of the portion of the travel time residuals contributed by the event, ΔT_i^{res} ($\Delta T^{\text{res}} = \sum_i^N \Delta T_i^{\text{res}}$). ΔT_i^{res} is defined as

$$\Delta T_i^{\text{res}} = w_1 * \Delta T_{i,a} / N + w_2 * \sum_j^{M_i} \Delta T_{i,j,r} / 2M + w_3 * \sum_j^{P_i} \Delta T_{i,j,c} / 2Q \quad (8)$$

where j is the event paired with event i , M_i the number of event pairs with differential travel time related to event i , and P_i the number of event pairs with coda cross-correlogram related to event i .

The relocation error of event i is defined as

$$e_i = \text{ellipse}[\min(\Delta T_i^{\text{res}}) * \chi^2(95, n)] \quad (9)$$

where $\chi^2(95, n)$ is the 95% confidence interval of chi-square distribution and n is the freedom of constraints.

Besides, three other types of uncertainties of earthquake location and origin time exist and are estimated in hypoRelocate, with one related to the method itself, one to possible travel time error in phase picking, and one to uneven distribution of seismic stations.

The standard bootstrap approach [Billings, 1994; Shearer, 1997; Waldhauser and Ellsworth, 2000] is adopted to estimate those uncertainties in hypoRelocate relocation. We introduce the general concept of the approach in this section and elaborate the details in the real data application in section 4.4. In the approach, we select a group of (M) events and repeat the relocation procedures a certain number (N) of times with some constraints randomly changed in each relocation and the relocation results from these repeated procedures form $M \times N$ bootstrap samples. The uncertainties are estimated from the distribution of these bootstrap samples, with the range that contains a certain percentage (e.g., 95%) of the samples defined as the uncertainties.

4. Application for Relocating the Aftershocks of Lushan Earthquake

On 20 April 2013, a magnitude M_w 6.6 earthquake occurred in Lushan, Sichuan province, the People's Republic of China (Lushan earthquake). The Lushan main shock and a large number of aftershocks are recorded by the dense seismic networks in the region. In this section, we apply hypoRelocate to relocate these events as an example of showing its practical application and discussing the effects of various constraints on the relocation results.

4.1. Traditional Constraints of Travel Time and Travel Time Difference

We use the event catalog and observed waveforms from 20 April to 29 June 2013 that are archived in the China Earthquake Networks Center. We select the main shock and 38 large aftershocks with M_l magnitude larger than 4.5 as the reference events (stars in Figure 5) and other 261 smaller aftershocks whose M_l magnitudes are between 3.0 and 4.5 (dots in Figure 5).

As S arrivals cannot be clearly picked in the data, only P phases are used in relocation. For absolute travel time, we use two different P phases, P_g and P_n , depending on the epicentral distance (Figure 6). The uncertainty of those P wave arrival picks is 0.1 s.

For travel time difference between the events, we pair the events whose interevent distance is less than 10 km according to the event catalog. There are 7510 event pairs among the relocated events, and a total of 87030 travel time differences are selected between these events. Every event has an average of 25 links with its neighbors, and every link has observations at a minimal of 5 stations (with an average of 12 stations). Each event pair has P_g travel time differences at 5 to 6 stations and P_n travel time differences at the rest of other stations. We first attend to obtain the travel time difference between the event pairs through cross correlation of the P waveforms. However, the waveforms are not alike between the event pairs, and most of correlation coefficients are lower than 0.4, due to the complex local velocity structure. We therefore obtain the differential travel times based on phase pick times.

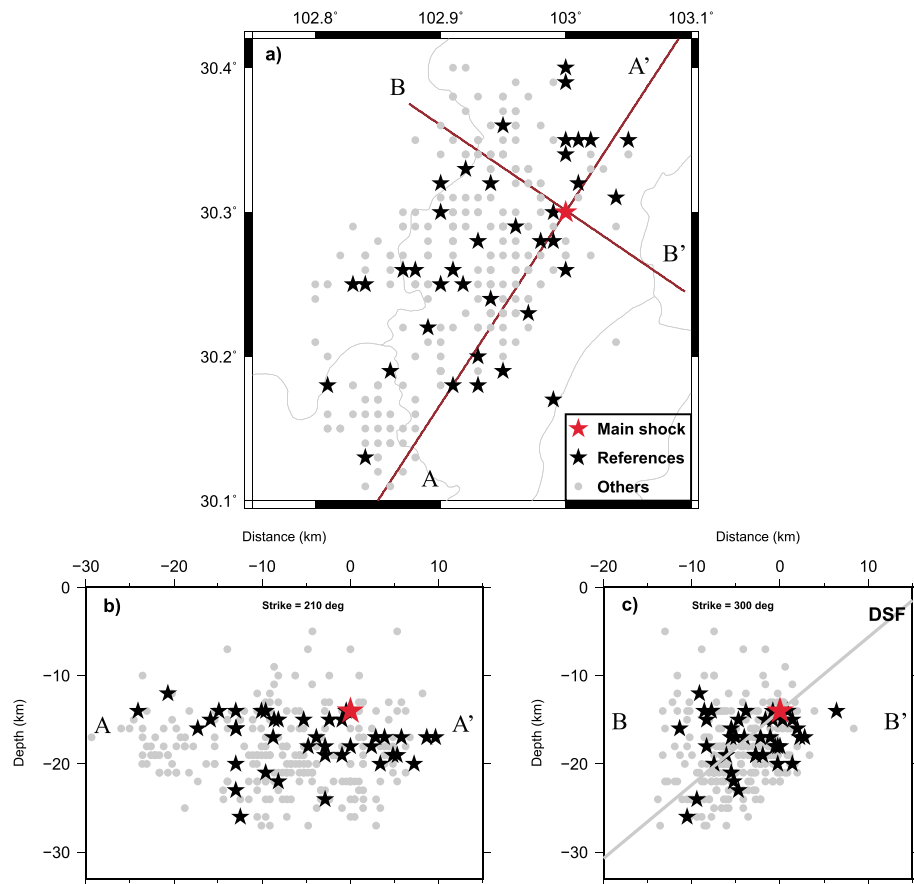


Figure 5. Earthquakes used in this study: (a) geographic distribution and distributions in cross-sectional views, with (b) along the fault strike (AA') and (c) perpendicular to the fault plane (BB'). Black stars are the reference events ($M_l > 4.5$), gray dots are other events ($4.5 > M_l > 3.0$), and red star is the main shock. The thick gray line in Figure 5c indicates the deduced seismic fault based on the Global Centroid Moment Tensor Catalog [Dziwonski et al., 1981; Ekström et al., 2012]. Event locations are based on the catalog of China Earthquake Networks Center.

4.2. Coda Cross-Correlogram Constraints on Interevent Distance of the Reference Events

Thirty-nine reference events (including the main shock) are well recorded by more than 50 seismic stations within 5° from the epicenters (Figure 6). The coda wave recorded in these stations are used for constructing coda cross-correlograms between the reference events, except for the main shock, in which only the data recorded at the stations from 3° to 5° are used due to clipping of the recording during the main shock in local seismic stations.

The procedures for constructing stacked coda correlogram are as follows: (1) the velocity seismic records are rotated to the tangential direction and band-pass filtered between 0.2 and 5 Hz, and (2) we use a 30 s sliding window with a moving time step of 10 s to cut the waveform between 20 s and 160 s after the predicted SH arrivals. The cross correlation is performed for every station and every time window between the events, and the cross-correlograms of all the stations are stacked for each time window (Figure 7). Figure 7a shows the cross-correlograms of event pair 16 and 44 at different station in one time period (70 s–100 s after S arrival) and the stacked result of all the stations (bottom trace, Figure 7a). Although no clear phase is visible in single cross-correlogram, one strong phase appears around -3 s after the stacking. Two sharp spikes emerge on the stacked cross-correlogram over 12 time periods of the coda waves (bottom trace, Figure 7b).

Due to seismic noise and other factors as we showed in the synthetic tests, not every stacked cross-correlogram would show clear energy spikes. After high signal to noise ratio autoselection and visual inspection of quality, we are able to obtain 151 clear stacked coda cross-correlograms between event pairs among those 39 reference events (Figures 8 and 9). Among them, 10 coda cross-correlograms exhibit symmetric

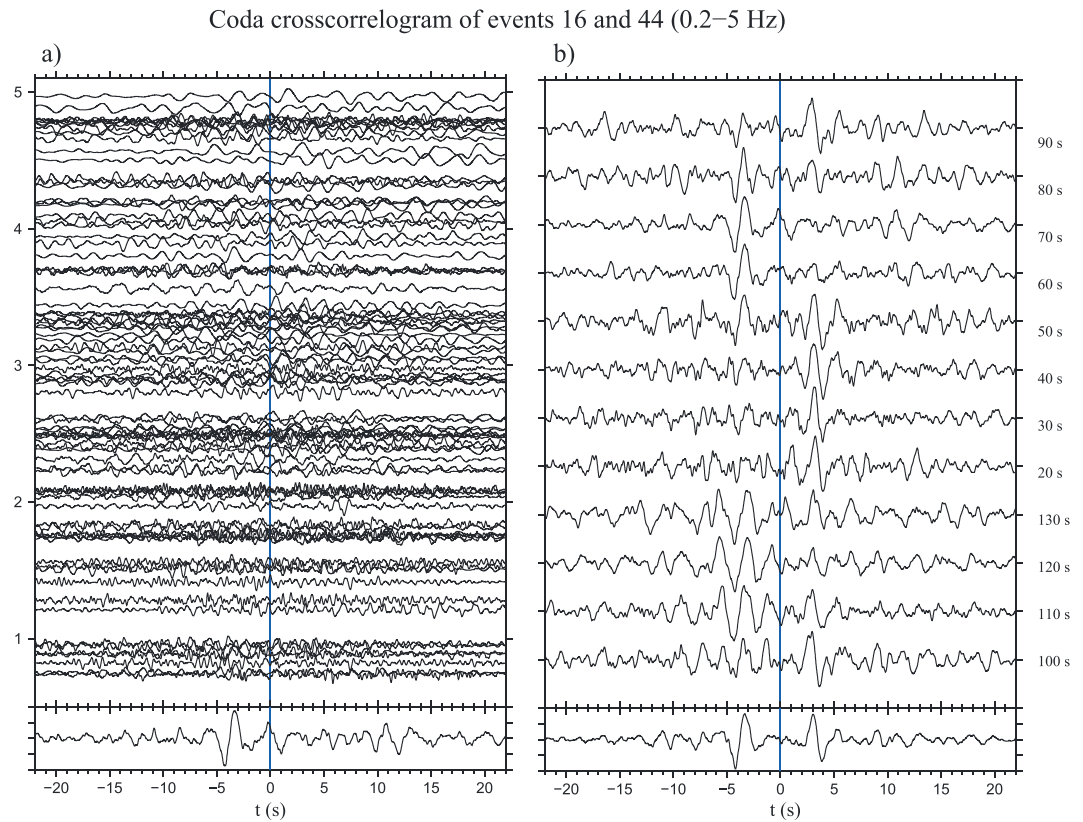


Figure 7. Examples of coda cross-correlogram between event pair 16 and 44 (events connected by the red line in Figure 8). (a) (top) Coda cross-correlograms obtained at individual stations within the epicenter distances from 0° to 5° , for the coda waves in the time window from 70 s to 100 s after the predicted S wave arrival time, (bottom) the stacked cross-correlogram of those in the top panel; (b) (top) the stacked cross-correlograms for the coda waves in different time windows. Each time window is 30 s long, and the starting time of the window is labeled on the right of each trace (seconds after the predicted S wave arrival), (bottom) the stacked cross-correlogram over the traces in the top panel.

time of the maximal amplitude still accurately reflects the travel time of the direct S wave between the events; we thus measure the travel time based on the absolute peak amplitude in the coda cross-correlograms.

4.3. Velocity Model

Lushan aftershocks occurred on the Longmenshan fault, which separates the Tibet Plateau in the west from the Chengdu plain in the east. Thus, there is significant difference in crustal structure between the two sides of the fault, and the lateral variation of velocity structure needs to be accurately accounted for in the relocation. Two models have been used in previous studies of earthquake relocations in the region. *Huang et al.* [2008] adopted a model with two one-dimensional models (Table 1) for each side of the fault in relocation of the Wenchuan earthquake and aftershocks. Their model was derived from seismic exploration lines and modeling natural seismic recordings. *Fang et al.* [2013] used two velocity models in their study of Lushan main shock and aftershocks, with one model similar to the model of *Huang et al.* [2008] and the other model derived from deep seismic sounding. Events are relocated with all these models. We eventually choose the model in *Huang et al.* [2008] (Table 1 and the heavy line in Figure 6 for the geographical separation of the two sides), because it generates the smallest residual value in the best fitting relocation results. The predicted travel times are calculated by ray tracing method according to the models.

4.4. Relocation Results and Uncertainties

In the relocation, we use 7697 absolute travel times (Pg and Pn phases), 87,030 pairs of differential travel time and 151 coda cross-correlograms. The initial searching area of event location is chosen to be a region of 0.2° in latitude, 0.2° in longitude, and 15 km in depth, centered at the catalog location of each event, and the initial searching range of event origin time is chosen to be ± 6 s from the catalog origin time. We test

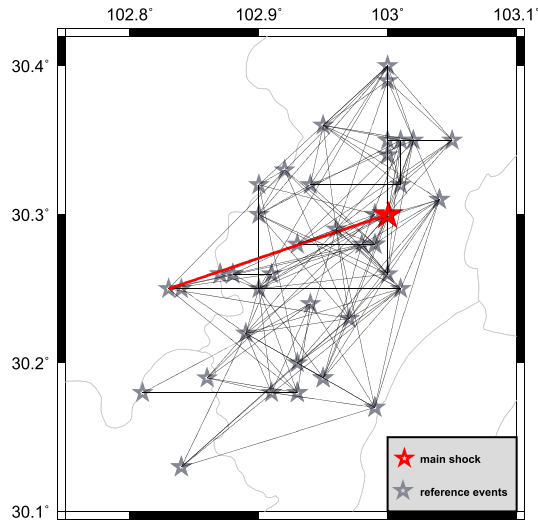


Figure 8. The 151 event pairs (connected by thin lines) with cross-correlogram constraint. Gray stars indicate 39 reference events (including the main shock, red star) with event ID labeled nearby. Cross-correlograms between event pair 16 and 44 (connected by thick red line) is presented as an example in Figure 7.

many cooling rates and the associated convergence of the solution in the simulated annealing method. We show the procedure performance in Figure 10, using two example cooling rates. Note that the procedure can provide similar convergent results (defined when the total residual changes by no more than 0.1% between the iterations) using either cooling rate, but the maximum number of iteration differs between the two cooling rates (Figure 10). After testing, we choose a cooling rate of 0.98 and a maximal number of iteration of 800.

The weighting factors are chosen depending on the quality of the data sets and the relative importance the constraint plays in constraining the model parameters. In principal, we give high-precision data a larger weighting factor and less accurate data a smaller one; we also place emphasis on the relative locations of events in the relocation results. Coda cross-correlogram data are regarded as having the highest precision and placing the most important constraints on the interevent distances. So we give that type of the constraint the largest weighting factor. Differential travel time and absolute travel time are both measured from the catalog phase data and have same precisions, but differential travel time is less sensitive to the velocity model and places stronger constraints on the relative location between the events. Therefore, we give it a larger weight than the absolute time.

The weighting factors are chosen depending on the quality of the data sets and the relative importance the constraint plays in constraining the model parameters. In principal, we give high-precision data a larger weighting factor and less accurate data a smaller

Coda Crosscorrelogram Examples (0.2–5 Hz)

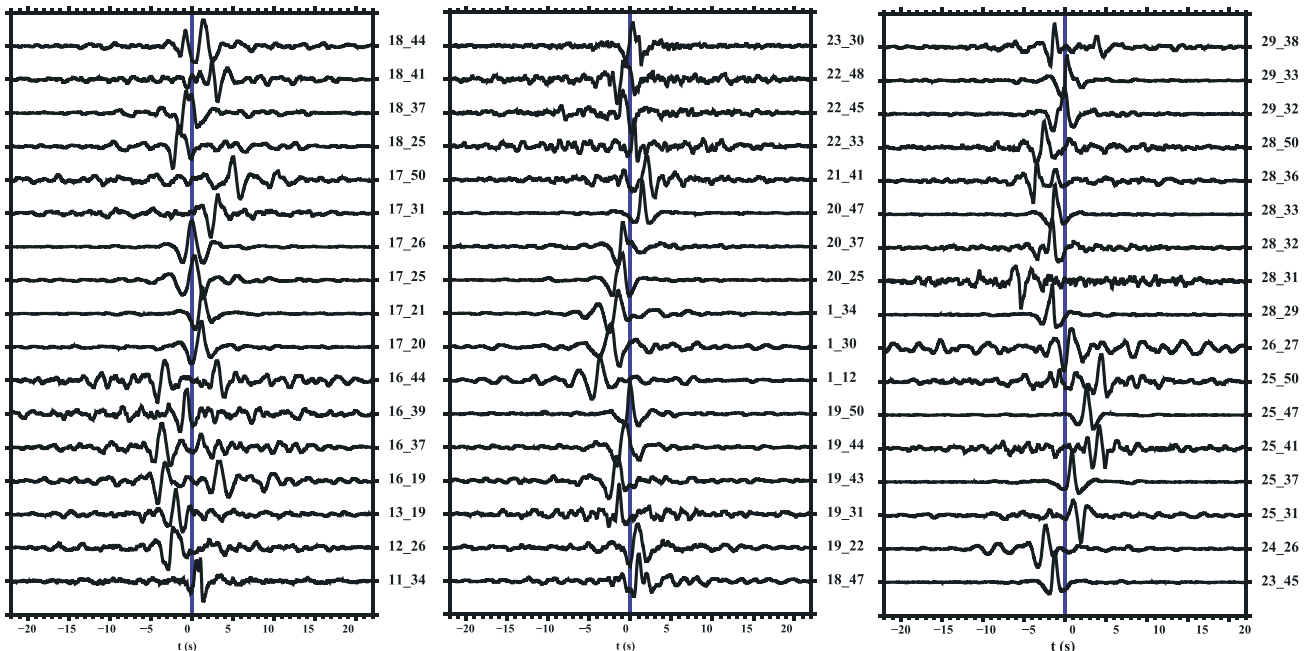


Figure 9. Examples of the stacked coda cross-correlograms from 151 event pairs, with the pair of event IDs (shown in Figure 8) labeled on the right of each trace. The blue lines mark the zero time.

Table 1. Velocity Model Used for Relocation

Westside P/S Ratio 1.68		Eastside P/S Ratio 1.78	
V_p (km/s)	Depth (km)	V_p (km/s)	Depth (km)
5.20	0.0	4.35	0.0
6.03	2.0	5.85	3.0
7.25	28.0	6.80	18.0
7.90	64.0	8.40	41.0
8.10	75.0	8.60	60.0

In reality, we also choose the weighting factors based on the relocation residuals when only each individual type of constraint is used. We first relocate all events with only each type of the constraint used and obtain the smallest residuals of the three kinds of constraints when each of them is used as the sole constraint.

Then, we combine the three constraints into relocation and adjust the weighting factors. The final weighting factors are chosen so that the residual related to the coda cross-correlogram is the smallest while the residuals related to other two types of constraints are no more than 10% of the smallest residuals when they are used solely in the relocations. Following these principles and procedures, we choose the final weighting factors of 0.7, 0.2, and 0.1 for coda cross-correlogram time, differential travel time, and absolute travel time, respectively. We should emphasize that as in the cases of any other joint inversions, those factors remain empirical. Users should consider each individual relocation case and choose weighting factors accordingly.

The relocation result is shown in map view and cross-section views in Figures 11a and 12a, respectively. The total residual is reduced from 1.07 s to 0.38 s, with the residuals associated with absolute time, differential travel time, and coda cross-correlogram decreasing by 0.28 s, 0.32 s, and 0.75 s, respectively (Table 2). The relocated events are moved shallower and become more spatially concentrated. Overall, the change of horizontal distance is relatively smaller than the change of event depth. The locations of 90% of the relocated events differ from the initial catalog by 1 to 3 km in horizontal distance (cf. Figures 5a, 11a, and 13a). In contrast, most of the event depths are changed by -15 to 5 km, with 50% of the events moved 5 to 10 km shallower (Figures 12a and 13b). Most of the events were located beneath the fault plane (deduced from global centroid moment tensor solution) in the catalog (Figures 5b and 5c), while most of the relocated events above the fault plane (Figure 12a). There are also a couple of events located out of the deduced fault (Figure 12a) (the locations of these events are well resolved in the relocation).

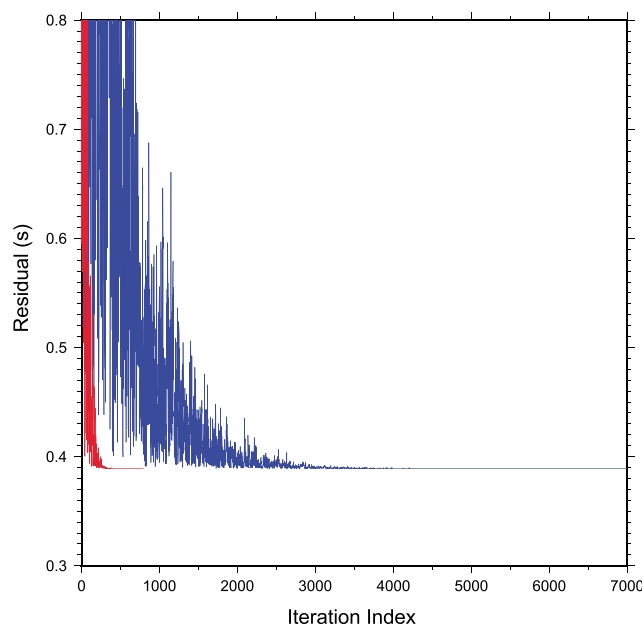


Figure 10. Total travel time residual as a function of iteration index in the simulated annealing method, for two example cooling rates (blue curve for a cooling rate of 0.998 with a maximum number of iteration of 7000 and the red curve for a cooling rate of 0.98 with a maximum number of iteration of 800).

Then, we combine the three constraints into relocation and adjust the weighting factors. The final weighting factors are chosen so that the residual related to the coda cross-correlogram is the smallest while the residuals related to other two types of constraints are no more than 10% of the smallest residuals when they are used solely in the relocations. Following these principles and procedures, we choose the final weighting factors of 0.7, 0.2, and 0.1 for coda cross-correlogram time, differential travel time, and absolute travel time, respectively. We should emphasize that as in the cases of any other joint inversions, those factors remain empirical. Users should consider each individual relocation case and choose weighting factors accordingly.

The relocation result is shown in map view and cross-section views in Figures 11a and 12a, respectively. The total residual is reduced from 1.07 s to 0.38 s, with the residuals associated with absolute time, differential travel time, and coda cross-correlogram decreasing by 0.28 s, 0.32 s, and 0.75 s, respectively (Table 2). The relocated events are moved shallower and become more spatially concentrated. Overall, the change of horizontal distance is relatively smaller than the change of event depth. The locations of 90% of the relocated events differ from the initial catalog by 1 to 3 km in horizontal distance (cf. Figures 5a, 11a, and 13a). In contrast, most of the event depths are changed by -15 to 5 km, with 50% of the events moved 5 to 10 km shallower (Figures 12a and 13b). Most of the events were located beneath the fault plane (deduced from global centroid moment tensor solution) in the catalog (Figures 5b and 5c), while most of the relocated events above the fault plane (Figure 12a). There are also a couple of events located out of the deduced fault (Figure 12a) (the locations of these events are well resolved in the relocation).

The relocation errors of the absolute location of the reference events are estimated based on equations (8) and (9), to be around 1 km in horizontal direction and 1–2 km in depth (Figures 11a and 12a). The relocation errors of other smaller events are about 1.5 times of those of the reference events due to the lack of constraint from coda cross-correlograms. The estimation of other uncertainties follows the bootstrap method illustrated in section 3.3. Thirty-nine reference events are selected for the uncertainty estimations (black stars in Figure 5 and crosses in Figures 11 and 12).

Owing to the random procedure in the simulated annealing method, the relocation results would have slight difference, if we repeat the procedure. To estimate the uncertainty of the simulated annealing method, we simply repeat the relocation procedures

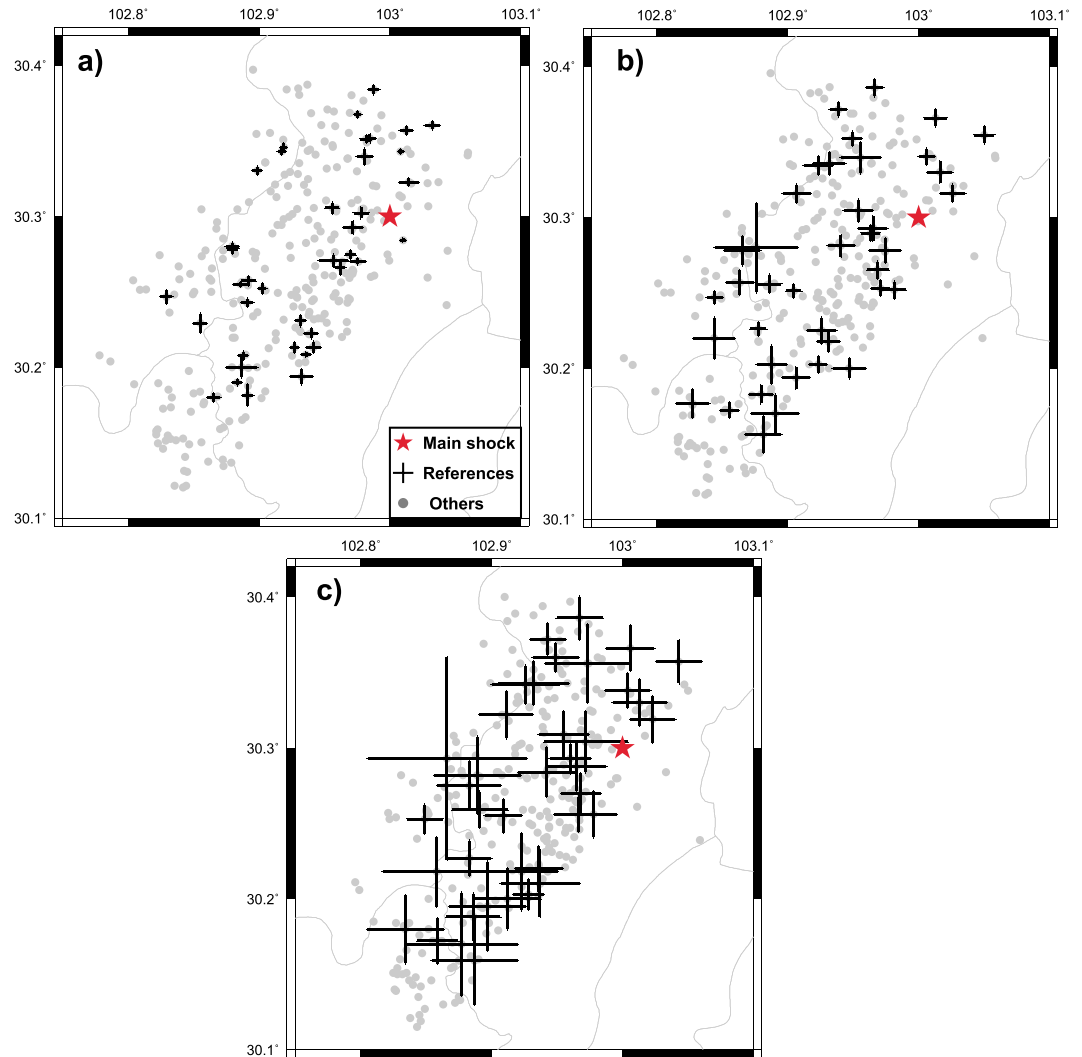


Figure 11. Map views of relocation results using various constraints based on different methods: (a) case 1: using constraints of coda cross-correlogram, absolute travel time, and travel time difference based on hypoRelocate; (b) case 2: using constraints of absolute travel time and travel time difference based on hypoRelocate; and (c) case 3: using constraints of travel time difference based on hypoDD. Black crosses are the reference events ($M_l > 4.5$) (The lengths of the two axes of the crosses indicate the location errors in longitude and latitude directions that estimated by the 95% chi-square distribution of the relocation residual and the size of the crosses are equal proportion to the basemap.), gray dots other events ($4.5 > M_l > 3.0$) and red star the main shock.

200 times with the same data constraints. The bootstrap samples thus contain 39 events in 200 times of repeated relocation procedures (200×39 samples). The location of an individual event in each relocation is plotted with respect to the averaged location of that individual event obtained in the 200 repeated times. The ellipses that include 95% of all sample points are regarded as the uncertainties of the relocation results. The estimated uncertainties for the simulated annealing method itself are 0.1 km in both horizontal and vertical locations (Figures 14a and 14b) and 0.01 s in event origin time (Figure 14c). To estimate the uncertainty associated with the travel time error in phase picking, for each repeated relocation, we randomize the travel time residuals of individual stations of the best fitting model and add them back to the travel time observations of all the stations. The uncertainties due to phase pick error are 0.2 km in the horizontal distance (Figure 14d), 0.25 km in depth (Figure 14e), and 0.04 s in event origin time (Figure 14f). To estimate the uncertainty associated with possible bias of station distribution, for each repeated relocation, we randomly pick 70% of the stations from the current station list. The uncertainties are 0.3 km in the horizontal distance (Figure 14g), 0.32 km in depth (Figure 14h), and 0.06 s in event origin time (Figure 14i) due to possible bias in station distribution.

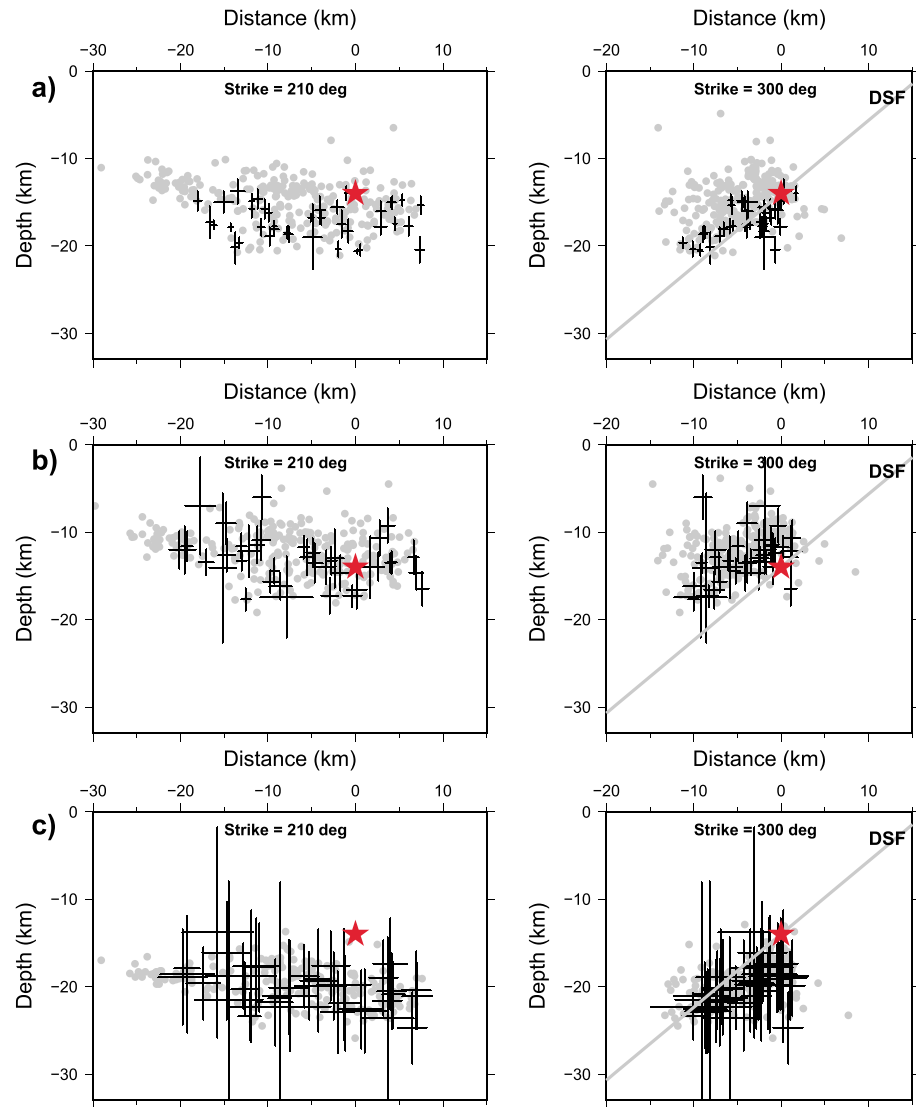


Figure 12. (a–c) Same as Figure 11, except in cross-sectional views, with the left panels along AA' and the right panels along BB' (profiles shown in Figure 5). Gray thick lines in the right panels are the same fault lines in Figure 5c.

5. Comparison of the Relocation Results With Different Constraints and With HypoDD

To illustrate the effect of different types of constraint, we compare the above relocation results (case 1) with another two cases with different types of constraint and different methods: case 2: absolute travel time and travel time difference are used and hypoRelocate is employed (Figures 11b and 12b); case 3: only travel time difference is used and hypoDD program [Waldhauser, 2001] is employed (Figures 11c and 12c).

The differences of horizontal locations of the relocated events are small between these cases, with 90% of the relocated events within 1 km between cases 1 and 2 (Figures 11a and 11b) and within 2 km between cases 1 and 3 (Figures 11a and 11c). However, larger differences exist in event depth. The relocated events are concentrated in the depth range between 15 and 25 km in case 3 (Figure 12c) that is similar to catalog depths (Figure 5b), 10–20 km in case 1 (Figure 12a) and 8–18 km in case 2 (Figure 12b). Events are located beneath the fault in case 3 (Figure 12c), while they are distributed on the top surface of the fault in cases 1 and 2 (Figures 12a and 12b). HypoDD in case 3 only uses travel time difference, which places constraints on the relative locations between the events, so the absolute locations of the relocated events would still depend on the initial catalog (The west velocity model is used in hypoDD relocation, because all the sources are located on

Table 2. Residuals for the Catalog and the Cases in Figures 11 and 12^a

Case	Constraint	Average Residual			ΔT^{res} Total residual (s)
		$\Delta T_{i,a}$ Absolute Travel Time (s)	$\Delta T_{i,j,r}$ Differential Travel Time (s)	$\Delta T_{i,j,c}$ Coda Cross-Correlogram (s)	
Case 1	a, d, c	0.66	0.42	0.33	0.38
Case 2	a, c	0.63	0.39	0.45	0.46
Case 3	d	0.75	0.46	0.56	0.56
Catalog	N/A	0.92	0.74	1.18	1.07

^aThe a, d, and c in column of “constraint” stand for absolute travel time, differential travel time, and coda cross-correlogram, respectively.

the westside and differential travel times are sensitive only to the velocity structure in the source regions.). That is the reason that the event depths in case 3 are similar to the catalog depths. The difference between cases 2 and 3 is mostly due to the additional constraint of absolute travel time data in case 2, which changes most of the event depths from the catalog values. Note that case 3 yields a large residual in absolute travel time (Table 2), which indicates that the absolute event locations in the catalog have large uncertainties. The relocation error bars decrease as more constraints are added into the relocation (Figures 11 and 12), indicating the improvement of relocation results with combined constraints.

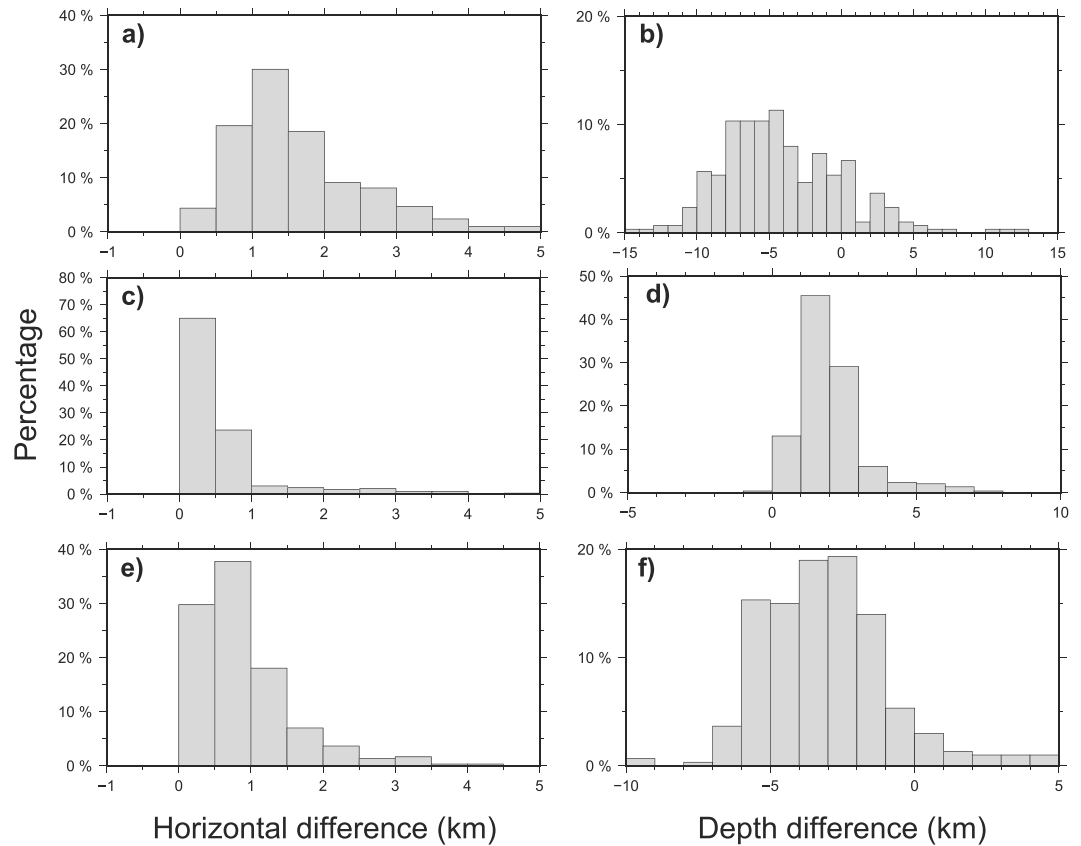


Figure 13. Statistics of location differences between different relocation cases, with Figures 13a, 13c, and 13e for the difference in horizontal distance and Figures 13b, 13d, and 13f for the depth difference: (a, b) between hypoRelocate relocation results (case 1 in section 5, Figures 11a and 12a) and the initial catalog (Figure 5), (c, d) between hypoRelocate results with (case 1 in section 5, Figures 11a and 12a) and without (case 2 in section 5, Figures 11b and 12b) constraints of coda cross-correlogram (both relocations have constraints of travel time and travel time difference), and (e, f) between hypoRelocate relocation results (case 1 in section 5, Figures 11a and 12a) and hypoDD results (case 3 in section 5, Figures 11c and 12c).

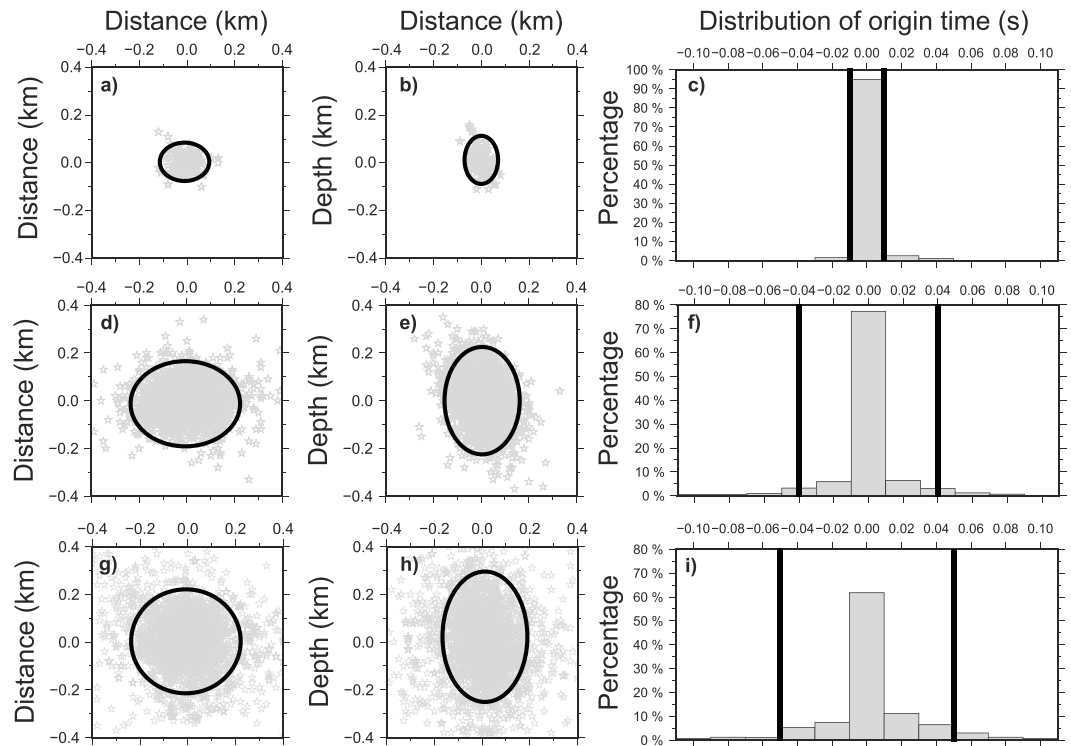


Figure 14. Distribution and uncertainties of hypoRelocate results of the reference events of Lushan earthquake sequence in bootstrap analyses: due to the simulated annealing method itself with (a) for location in map view, (b) for location in north-south cross-sectional view, and (c) for event origin time; (d–f) same as Figures 14a–14c, except due to possible phase pick error; (g–i) same as Figures 14a–14c, except due to possible biased station distribution. Bootstrap samples contain 39 reference events that are relocated 200 times. Event locations and origin times are plotted with respect to the averages (0, 0) of all the relocations. Black ellipses in the location plots (Figures 14a, 14b, 14d, 14e, 14g, and 14h) and black thick lines in event origin time plots (Figures 14c, 14f, and 14i) contain 95% of the samples from the distributions and are considered as relocation errors.

Because hypoDD only employs travel time difference that is only sensitive to the relative location between the events, its relocation results would be affected by the initial event catalog. There are some previous studies that combined absolute travel time and differential travel time together to improve relocation precision [Jordan and Sverdrup, 1981; Engdahl and Bergman, 2001]. One approach to improve the accuracy of the relocation results is to first redetermine the absolute locations of the events using a traditional method [Klein, 2002] and a good regional velocity model and then to employ hypoDD to improve the accuracy of the relative location of the events by applying differential constraints in further relocation [Fang *et al.*, 2013]. In case 1, hypoRelocate incorporates the absolute travel time into joint inversion. This serves the same purpose as the two-step approach adopted by others, but it also ensures the consistency between the best fitting locations and the minimization of the absolute travel time residuals. It is also interesting to note that the relative travel time residual is smaller in cases 1 and 2 than in case 3 (Table 2), suggesting that more accurate absolute locations would also yield better fitting relative locations.

The results in cases 1 and 2 are similar (Figures 12a, 12b, and 13d), but some difference exists in the reference events. The reference events are all located above the fault in case 2 (Figure 12b) but along the fault in case 1 (Figure 12a). This difference of relocation results is due to the additional constraint from coda cross-correlograms in case 1. The residuals related to absolute time and relative travel time are slightly larger in case 1 than those in case 2 (Table 2), but the residual related to cross-correlogram is reduced from 0.45 s in case 2 to 0.33 s in case 1.

We further illustrate the effects of the additional constraint of coda cross-correlograms on the determined event location, using a pair of reference events (events 20 and 25 in Figure 8) (Figure 15) and the reference events (Figure 16) as examples. We show results for two cases, with one using only the travel time difference

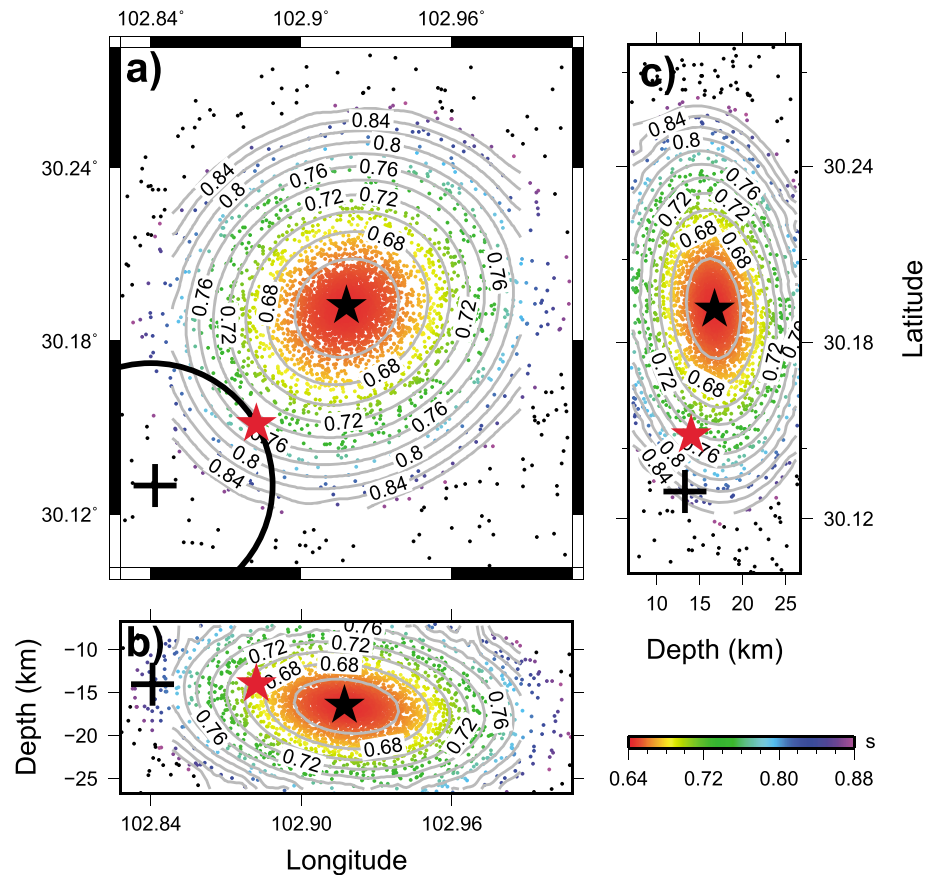


Figure 15. Determined relative locations of a relocated event (event 25 in Figure 8, stars) with respect to the reference event (event 20 in Figure 8, cross) for two cases. Case 1 (black star): only the travel time difference between the events is used; case 2 (red star): both the travel time difference and stacked coda cross-correlogram are used as constraints. The residual of differential travel time as a function of event location is represented by background color and gray contours, while the thick black circle in Figure 15a is the interevent distance constrained based on the cross-correlogram. (a) Map view, (b) cross-sectional view in longitude versus depth, and (c) cross-sectional view in latitude versus depth.

as constraint and the other employing the travel time difference and the constraint of coda cross-correlogram between the events. In the example of an event pair (Figure 15), one event is fixed in its location and origin time (cross symbol) and the other event is relocated with respect to the fixed event. The color maps and isolines show the residuals of travel time difference of the *P* waves between the events. If only the travel time difference is used in the relocation, the relocated event will be placed at the minimum value of residuals (black star). The thick black circle centered at the fixed event is the potential location of the relocated event based on the stacked coda cross-correlogram (i.e., it has a radius of inter-event distance determined based on the stacked coda cross-correlogram). If both the travel time difference and cross-correlogram information are used, the constrained location is placed at the minimum value of the weighed residual as defined in equation (1) (red star). The two relocation results differ by 5.6 km in the horizontal distance and 2.7 km in depth. Note that the residuals related to the travel time difference between the two relocation results are less than 0.08 s, rather insignificant in comparison with the precision of the travel-time time difference in the present study (larger than 0.1 s). The additional constraint of the coda cross-correlogram between the events places much tighter constraints on the relative location of the events. In the example of the reference events (Figure 16), we compare reference event locations in two different relocation cases: (1) hypoDD employing differential travel time only and (2) hypoRelocate utilizing both differential travel time and coda cross-correlogram. The differences of the two relocation results are obvious both in horizontal and depth directions (Figure 16). More than a half of the events have a 2–4 km horizontal separation (Figure 16a), and most of the events move shallower after adding the constraint of coda cross-correlogram (Figures 16b and 16c). The depths of some events vary as much as 5 km. While the average

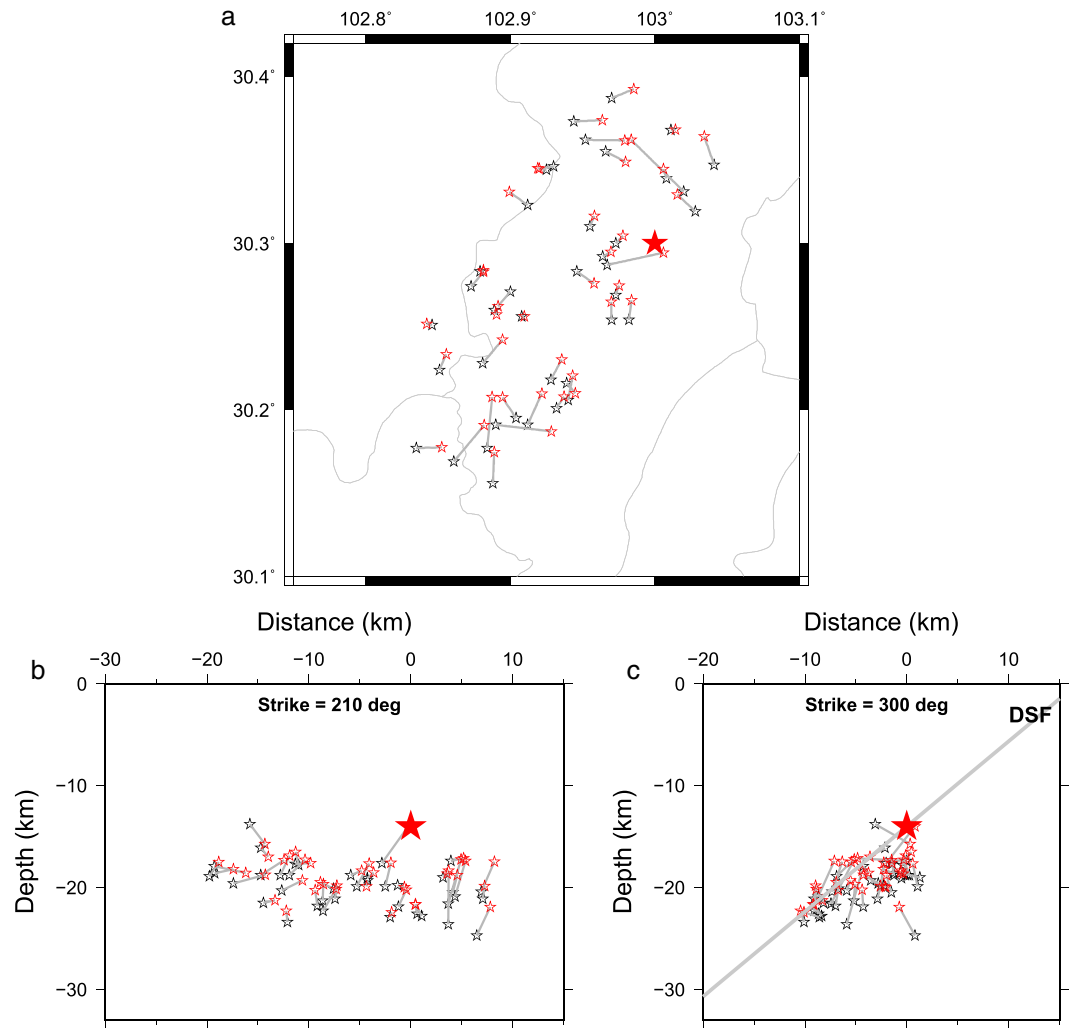


Figure 16. The comparison of reference event locations between two relocation cases: hypoRelocate employing both differential travel time and coda cross-correlogram (small red triangles) and hypoDD employing differential travel time only (black triangles). (a–c) Subplots have the same base maps as Figures 5a–5c. The thin gray lines link the same event between the two cases.

residuals associated with the differential travel time vary slightly from 0.47 s to 0.51 s between the two cases, the average residuals associated with the cross-correlogram drop from 0.55 s to 0.39 s from case 1 to case 2. The above comparisons indicate that the additional constraint of coda correlogram places much tighter constraint on the relative locations between the events.

6. Conclusion

We develop a new method hypoRelocate to determine high-resolution earthquake location based on constraints of coda cross-correlogram, traditional absolute travel time, and differential travel time of seismic phases between the events. The relocation is performed by using the simulated annealing method to search for the best fitting locations and origin times of the events that minimize the total residual of the constraints. Coda cross-correlogram is demonstrated to be able to provide accurate constraints on interevent distance between events and is introduced in the first time into earthquake relocation. HypoRelocate expands the advantage of using differential constraints to determine high-resolution relative locations between the events by employing additional constraints of coda cross-correlograms and reduces the dependence of relocation results on the accuracy of the initial catalog by incorporating the absolute time into the joint inversion.

We apply the method to relocate the aftershocks of Lushan earthquake, including the main shock and 38 large aftershocks with a magnitude (M_i) larger than 4.5 as the reference events and 261 other smaller aftershocks. The relocation result clearly depicts a seismic fault profile that is consistent with the one deduced from the GCMT solution. Most of the aftershocks are located between depths from 10 to 20 km and are distributed in the hanging wall. There are few events shallower than 10 km, indicating that the main shock did not rupture to the surface, consistent with the field observations. Comparisons of the relocation results between hypoRelocate and hypoDD, a high-resolution relocation program using differential travel time between the events, indicate that the additional constraints of coda cross-correlogram and absolute travel time place tighter constraints on both the event depth and relative location between the events.

Acknowledgments

We acknowledge the China Earthquake Networks Center for providing seismic data (<http://www.csndmc.ac.cn/new-web/>) and GMT for mapping tool (<http://gmt.soest.hawaii.edu/>). The source code for hypoRelocate can be downloaded from <http://seis.ustc.edu.cn/HypoRelocate/>. We thank Eric Bergman, Andrew Curtis, and one anonymous reviewer for providing comments that have significantly improved the paper. This work was supported by the National Natural Science Foundation of China under grant NSFC41130311 and the Chinese Academy of Sciences and State Administration of Foreign Experts Affairs International Partnership Program for Creative Research Teams.

References

- Aki, K. (1969), Analysis of the seismic coda of local earthquakes as scattered waves, *J. Geophys. Res.*, *74*(2), 615–631, doi:10.1029/JB074i002p00615.
- Aki, K., and B. Chouet (1975), Origin of coda waves: source, attenuation, and scattering effects, *J. Geophys. Res.*, *80*(23), 3322–3342, doi:10.1029/JB080i023p03322.
- Billings, S. D. (1994), Simulated annealing for earthquake location, *Geophys. J. Int.*, *118*(3), 680–692.
- Bokelmann, G. H., and H. P. Harjes (2000), Evidence for temporal variation of seismic velocity within the upper continental crust, *J. Geophys. Res.*, *105*(B10), 23,879–23,894, doi:10.1029/2000JB900207.
- Bouchon, M., H. Karabulut, M. Aktar, S. Özalaybey, J. Schmittbuhl, and M.-P. Bouin (2011), Extended nucleation of the 1999 M_w 7.6 Izmit earthquake, *Science*, *331*(6019), 877–880.
- Campillo, M., and A. Paul (2003), Long-range correlations in the diffuse seismic coda, *Science*, *299*(5606), 547–549.
- Curtis, A., H. Nicolson, D. Halliday, J. Trampert, and B. Baptie (2009), Virtual seismometers in the subsurface of the Earth from seismic interferometry, *Nat. Geosci.*, *2*(10), 700–704.
- Dziewonski, A., T. A. Chou, and J. Woodhouse (1981), Determination of earthquake source parameters from waveform data for studies of global and regional seismicity, *J. Geophys. Res.*, *86*(B4), 2825–2852, doi:10.1029/JB086iB04p02825.
- Ekström, G., M. Nettles, and A. Dziewoński (2012), The global CMT project 2004–2010: Centroid-moment tensors for 13,017 earthquakes, *Phys. Earth Planet. Inter.*, *200*, 1–9.
- Ellsworth, W. L. (2013), Injection-induced earthquakes, *Science*, *341*(6142), 1225942.
- Engdahl, E., and E. A. Bergman (2001), Validation and generation of reference events by cluster analysis, *Rep., DTIC Document*.
- Fang, L., J. Wu, W. Wang, Z. Lü, C. Wang, T. Yang, and Y. Cai (2013), Relocation of the main shock and aftershock sequences of M 5.7.0 Sichuan Lushan earthquake, *Chin. Sci. Bull.*, *58*(28–29), 3451–3459.
- Furumoto, M., Y. Ichimori, N. Hayashi, Y. Hiramatsu, and T. Satoh (2001), Seismic wave velocity changes and stress build-up in the crust of the Kanto-Tokai region, *Geophys. Res. Lett.*, *28*(19), 3737–3740, doi:10.1029/2001GL013172.
- Galettis, E., and A. Curtis (2012), Generalised receiver functions and seismic interferometry, *Tectonophysics*, *532*, 1–26.
- Goffe, W. L., G. D. Ferrier, and J. Rogers (1994), Global optimization of statistical functions with simulated annealing, *J. Econ.*, *60*(1), 65–99.
- Gomberg, J. S., K. M. Shedlock, and S. W. Roecker (1990), The effect of S -wave arrival times on the accuracy of hypocenter estimation, *Bull. Seismol. Soc. Am.*, *80*(6A), 1605–1628.
- Hauksson, E., and P. Shearer (2005), Southern California hypocenter relocation with waveform cross-correlation, part 1: Results using the double-difference method, *Bull. Seismol. Soc. Am.*, *95*(3), 896–903.
- Hauksson, E., W. Yang, and P. M. Shearer (2012), Waveform relocated earthquake catalog for southern California (1981 to June 2011), *Bull. Seismol. Soc. Am.*, *102*(5), 2239–2244.
- Hoshihara, M. (1991), Simulation of multiple-scattered coda wave excitation based on the energy conservation law, *Phys. Earth Planet. Inter.*, *67*(1), 123–136.
- Huang, Y., J. Wu, T. Zhang, and D. Zhang (2008), Relocation of the M 8.0 Wenchuan earthquake and its aftershock sequence, *Sci. China Ser. Earth Sci.*, *51*(12), 1703–1711.
- Husen, S., and R. B. Smith (2004), Probabilistic earthquake relocation in three-dimensional velocity models for the Yellowstone National Park region, Wyoming, *Bull. Seismol. Soc. Am.*, *94*(3), 880–896.
- Jordan, T. H., and K. A. Sverdrup (1981), Teleseismic location techniques and their application to earthquake clusters in the south-central Pacific, *Bull. Seismol. Soc. Am.*, *71*(4), 1105–1130.
- Kato, A., K. Obara, T. Igarashi, H. Tsuruoka, S. Nakagawa, and N. Hirata (2012), Propagation of slow slip leading up to the 2011 M_w 9.0 Tohoku-Oki earthquake, *Science*, *335*(6069), 705–708.
- Klein, F. W. (2002), User's guide to HYPOINVERSE-2000, a Fortran program to solve for earthquake locations and magnitudes *Rep. 2331–1258*, US Geological Survey.
- Lin, G., and P. Shearer (2005), Tests of relative earthquake location techniques using synthetic data, *J. Geophys. Res.*, *110*, B04304, doi:10.1029/2004JB003380.
- Lin, G., P. M. Shearer, and E. Hauksson (2007), Applying a three-dimensional velocity model, waveform cross correlation, and cluster analysis to locate southern California seismicity from 1981 to 2005, *J. Geophys. Res.*, *112*, B12309, doi:10.1029/2007JB004986.
- Long, H., and L. Wen (2012), Using repeated sources to quantitatively determine temporal change of medium properties: Theory and an example, *J. Geophys. Res.*, *117*, B09303, doi:10.1029/2012JB009302.
- Majer, E. L., R. Baria, M. Stark, S. Oates, J. Bommer, B. Smith, and H. Asanuma (2007), Induced seismicity associated with enhanced geothermal systems, *Geothermics*, *36*(3), 185–222.
- Martini, F., C. J. Bean, G. Saccorotti, F. Viveiros, and N. Wallenstein (2009), Seasonal cycles of seismic velocity variations detected using coda wave interferometry at Fogo volcano, São Miguel, Azores, during 2003–2004, *J. Volcanol. Geotherm. Res.*, *181*(3), 231–246.
- Matoza, R. S., P. M. Shearer, G. Lin, C. J. Wolfe, and P. G. Okubo (2013), Systematic relocation of seismicity on Hawaii Island from 1992 to 2009 using waveform cross correlation and cluster analysis, *J. Geophys. Res. Solid Earth*, *118*, 2275–2288.
- Miyazawa, M., R. Snieder, and A. Venkataraman (2008), Application of seismic interferometry to extract P - and S -wave propagation and observation of shear-wave splitting from noise data at Cold Lake, Alberta, Canada, *Geophysics*, *73*(4), D35–D40.
- Pavlis, G. L. (1992), Appraising relative earthquake location errors, *Bull. Seismol. Soc. Am.*, *82*(2), 836–859.

- Poliannikov, O. V., A. E. Malcolm, H. Djikpesse, and M. Prange (2011), Interferometric hydrofracture microseism localization using neighboring fracture, *Geophysics*, *76*(6), WC27–WC36.
- Poupinet, G., W. Ellsworth, and J. Frechet (1984), Monitoring velocity variations in the crust using earthquake doublets: An application to the Calaveras Fault, California, *J. Geophys. Res.*, *89*(B7), 5719–5731, doi:10.1029/JB089iB07p05719.
- Ratdomopurbo, A., and G. Poupinet (1995), Monitoring a temporal change of seismic velocity in a volcano: Application to the 1992 eruption of Mt. Merapi (Indonesia), *Geophys. Res. Lett.*, *22*(7), 775–778, doi:10.1029/95GL00302.
- Richards-Dinger, K., and P. Shearer (2000), Earthquake locations in southern California obtained using source-specific station terms, *J. Geophys. Res.*, *105*(B5), 10,939–10,960, doi:10.1029/2000JB900014.
- Roux, P., K. G. Sabra, P. Gerstoft, W. Kuperman, and M. C. Fehler (2005), *P*-waves from cross-correlation of seismic noise, *Geophys. Res. Lett.*, *32*, L19303, doi:10.1029/2005GL023803.
- Rubin, A. M. (2002), Aftershocks of microearthquakes as probes of the mechanics of rupture, *J. Geophys. Res.*, *107*(B7), 2142, doi:10.1029/2001JB000496.
- Rubin, A. M., D. Gillard, and J.-L. Got (1999), Streaks of microearthquakes along creeping faults, *Nature*, *400*(6745), 635–641.
- Rutledge, J. T., and W. S. Phillips (2003), Hydraulic stimulation of natural fractures as revealed by induced microearthquakes, Carthage Cotton Valley gas field, east Texas, *Geophysics*, *68*(2), 441–452.
- Schaff, D. P., and P. G. Richards (2004), Repeating seismic events in China, *Science*, *303*(5661), 1176–1178.
- Shapiro, N. M., M. Campillo, L. Stehly, and M. H. Ritzwoller (2005), High-resolution surface-wave tomography from ambient seismic noise, *Science*, *307*(5715), 1615–1618.
- Shearer, P. M. (1997), Improving local earthquake locations using the L1 norm and waveform cross correlation: Application to the Whittier Narrows, California, aftershock sequence, *J. Geophys. Res.*, *102*, 8269–8283, doi:10.1029/96JB03228.
- Shearer, P., E. Hauksson, and G. Lin (2005), Southern California hypocenter relocation with waveform cross-correlation, part 2: Results using source-specific station terms and cluster analysis, *Bull. Seismol. Soc. Am.*, *95*(3), 904–915.
- Simpson, D., W. Leith, and C. Scholz (1988), Two types of reservoir-induced seismicity, *Bull. Seismol. Soc. Am.*, *78*(6), 2025–2040.
- Snieder, R. (2002), Coda wave interferometry and the equilibration of energy in elastic media, *Phys. Rev. E*, *66*(4), 046615.
- Snieder, R. (2004), Extracting the Green's function from the correlation of coda waves: A derivation based on stationary phase, *Phys. Rev. E*, *69*(4), 046610.
- Snieder, R. (2006), The theory of coda wave interferometry, *Pure Appl. Geophys.*, *163*(2–3), 455–473.
- Snieder, R., A. Grêt, H. Douma, and J. Scales (2002), Coda wave interferometry for estimating nonlinear behavior in seismic velocity, *Science*, *295*(5563), 2253–2255.
- Szu, H., and R. Hartley (1987), Fast simulated annealing, *Phys. Lett. A*, *122*(3), 157–162.
- Talwani, P., and S. Acree (1984), Pore pressure diffusion and the mechanism of reservoir-induced seismicity, *Pure Appl. Geophys.*, *122*(6), 947–965.
- Tonegawa, T., and K. Nishida (2010), Inter-source body wave propagations derived from seismic interferometry, *Geophys. J. Int.*, *183*(2), 861–868.
- Van Laarhoven, P. J., and E. H. Aarts (1987), *Simulated Annealing: Theory and Applications*, Springer Science & Business Media.
- Waldhauser, F. (2001), hypoDD—A program to compute double-difference hypocenter locations.
- Waldhauser, F., and W. L. Ellsworth (2000), A double-difference earthquake location algorithm: Method and application to the northern Hayward fault, California, *Bull. Seismol. Soc. Am.*, *90*(6), 1353–1368.
- Waldhauser, F., and D. P. Schaff (2008), Large-scale relocation of two decades of Northern California seismicity using cross-correlation and double-difference methods, *J. Geophys. Res.*, *113*, B08311, doi:10.1029/2007JB005479.
- Wen, L. (2006), Localized temporal change of the Earth's inner core boundary, *Science*, *314*(5801), 967–970.
- Wen, L., and H. Long (2010), High-precision location of North Korea's 2009 nuclear test, *Seismol. Res. Lett.*, *81*(1), 26–29.
- Zhang, M., and L. Wen (2013), High-precision location and yield of North Korea's 2013 nuclear test, *Geophys. Res. Lett.*, *40*, 2941–2946, doi:10.1002/grl.50607.
- Zhang, M., D. Tian, and L. Wen (2014), A new method for earthquake depth determination: Stacking multiple-station autocorrelograms, *Geophys. J. Int.*, *197*(2), 1107–1116.